


Fibroblast growth factor 9 (FGF9)-mediated neurodegeneration: Implications for progressive multiple sclerosis?

Katja Thümmler¹  | Claudia Wrzos² | Jonas Franz^{2,3,4,5} | Daniel McElroy¹ | John J. Cole¹ | Lorna Hayden¹ | Diana Arseni¹ | Friedrich Schwarz² | Andreas Junker^{2,6} | Julia M. Edgar¹ | Sebastian Kügler^{7,8} | Andreas Neef^{3,4,5,9} | Fred Wolf^{3,4,5,9,10} | Christine Stadelmann^{2,10} | Christopher Lington¹

¹School of Infection and Immunity, University of Glasgow, Glasgow, UK

²Institute for Neuropathology, University Medical Center Göttingen, Göttingen, Germany

³Max Planck Institute for Dynamics and Self-Organization, Göttingen, Germany

⁴Max Planck Institute for Multidisciplinary Sciences, Göttingen, Germany

⁵Göttingen Campus Institute for Dynamics of Biological Networks, University of Göttingen, Göttingen, Germany

⁶Department of Neuropathology, University Hospital Essen, Essen, Germany

⁷Institute for Neurology, University Medical Center Göttingen, Göttingen, Germany

⁸Center Nanoscale Microscopy and Physiology of the Brain (CNMPB), Göttingen, Germany

⁹Center for Biostructural Imaging of Neurodegeneration, Göttingen, Germany

¹⁰Cluster of Excellence Multiscale Bioimaging: From Molecular Machines to Network of Excitable Cells (MBExC), University of Goettingen, Göttingen, Germany

Correspondence

Christine Stadelmann, Institute for Neuropathology, University Medical Center Göttingen, Göttingen, Germany.
Email: cstadelmann@med.uni-goettingen.de

Funding information

This study was supported by the Gemeinnützige Hertie Stiftung (C.L. and C.S.), the Deutsche Forschungsgemeinschaft (DFG) transregional Collaborative Research Centers (CRCs) 43 “The brain as a target of inflammatory processes” and 274 “Checkpoints of CNS recovery” Project ID 408885537, the DFG under Germany’s Excellence Strategy (EXC 2067/1-390729940), the Deutsche Multiple Sklerose Gesellschaft (DMSG), the Ministry for Science and Education of Lower Saxony and the Volkswagen Foundation (“Niedersächsisches Vorab”) and the National Multiple Sclerosis Society (USA), to C.S. J.F. is

Abstract

Aims: Fibroblast growth factor (FGF) signalling is dysregulated in multiple sclerosis (MS) and other neurological and psychiatric conditions, but there is little or no consensus as to how individual FGF family members contribute to disease pathogenesis. Lesion development in MS is associated with increased expression of FGF1, FGF2 and FGF9, all of which modulate remyelination in a variety of experimental settings. However, FGF9 is also selectively upregulated in major depressive disorder (MDD), prompting us to speculate it may also have a direct effect on neuronal function and survival.

Methods: Transcriptional profiling of myelinating cultures treated with FGF1, FGF2 or FGF9 was performed, and the effects of FGF9 on cortical neurons investigated using a combination of transcriptional, electrophysiological and immunofluorescence microscopic techniques. The in vivo effects of FGF9 were explored by stereotactic injection of adeno-associated viral (AAV) vectors encoding either FGF9 or EGFP into the rat motor cortex.

Christine Stadelmann and Christopher Lington contributed equally.

This is an open access article under the terms of the [Creative Commons Attribution-NonCommercial-NoDerivs](https://creativecommons.org/licenses/by-nc-nd/4.0/) License, which permits use and distribution in any medium, provided the original work is properly cited, the use is non-commercial and no modifications or adaptations are made.

© 2023 The Authors. *Neuropathology and Applied Neurobiology* published by John Wiley & Sons Ltd on behalf of British Neuropathological Society.

supported by the Clinician Scientist Program of the CRC274; F.W. by VW Foundation (ZN2632), by the Deutsche Forschungsgemeinschaft (DFG, German Research Foundation) 436260547 in relation to NeuroNex (National Science Foundation 2015276), DFG (CRC 1286, 889; SPP 2205, 1782), the Leibniz Association (project K265/2019), the Ministry for Science and Culture of Lower Saxony, and the Max Planck Society; C.L. by Naomi Bramson Trust and Alexander von Humboldt-Stiftung; K.T. and C.L. by MS Society UK; L.H. and D.A. by a PhD studentship from Medical Research Scotland (PhD-1031-2016); D.M. by a PhD studentship from MS Society UK; and K.T. by TENOVUS Scotland.

Results: Transcriptional profiling of myelinating cultures after FGF9 treatment revealed a distinct neuronal response with a pronounced downregulation of gene networks associated with axonal transport and synaptic function. In cortical neuronal cultures, FGF9 also rapidly downregulated expression of genes associated with synaptic function. This was associated with a complete block in the development of photo-inducible spiking activity, as demonstrated using multi-electrode recordings of channel rhodopsin-transfected rat cortical neurons in vitro and, ultimately, neuronal cell death. Overexpression of FGF9 in vivo resulted in rapid loss of neurons and subsequent development of chronic grey matter lesions with neuroaxonal reduction and ensuing myelin loss.

Conclusions: These observations identify overexpression of FGF9 as a mechanism by which neuroaxonal pathology could develop independently of immune-mediated demyelination in MS. We suggest targeting neuronal FGF9-dependent pathways may provide a novel strategy to slow if not halt neuroaxonal atrophy and loss in MS, MDD and potentially other neurodegenerative diseases.

KEYWORDS

fibroblast growth factor 9, major depressive disorder, multiple sclerosis, neurodegeneration

INTRODUCTION

Neurodegeneration is the underlying cause of chronic disability in multiple sclerosis (MS), a chronic inflammatory demyelinating disease of the central nervous system (CNS) that affects over 2.5 million people worldwide [1]. Neuronal damage and loss are observed in many brain regions [2–4] and are associated with cognitive dysfunction, fatigue and depression, as well as contributing to multiple motor and sensory deficits [5, 6]. Yet, despite its clinical importance, our understanding of the mechanisms underlying neuronal pathology in MS remains incomplete. The general consensus is that neuronal pathology develops in response to the detrimental effects of inflammatory demyelination on the structural integrity of myelinated axons [7, 8]. However, recent studies suggest an alternative scenario in which neuronal pathology develops independently of demyelination [9–15], a situation in which neuronal pathology is posited to be a primary, as opposed to secondary event in disease development.

The pathomechanisms contributing to neuronal injury in this scenario are poorly understood, but based on our previous expression data from MS tissue, we speculated this may involve dysregulation of fibroblast growth factor (FGF) signalling as discussed in other neurodegenerative and neuropsychiatric disorders [16–21]. The mammalian FGF family consists of 18 ligands that signal via a small family of transmembrane receptor kinases encoded by four genes (*FGFR1*, *FGFR2*, *FGFR3* and *FGFR4*). FGF plays important roles during neurogenesis where it contributes to the regulation of glial and neuronal progenitor cell proliferation, migration, differentiation and survival. However, its functional significance in the adult CNS remains unclear, although several studies indicate it may support a variety of neuroprotective responses following ischemic or traumatic brain injury [22].

Expression of several FGF family members is increased in MS tissue suggesting FGF9 signalling also contributes to lesion development

Key points

- Multiple sclerosis and major depressive disorder have been associated with increased expression of FGF9 in affected brain regions.
- We now report FGF9 is neurotoxic, as it rapidly downregulates neuronal gene networks required to maintain synaptic function and axonal transport and compromises the survival of post-mitotic neurons.
- FGF9 overexpression in the rat cortex initiates primary neurodegeneration and ensuing myelin loss in vivo.

in this disease [20, 21, 23]. These include FGF2 and FGF9, which are upregulated at sites of ongoing tissue damage where they may either promote lesion development by inhibiting (re)myelination [20, 23] or alternatively induce a neuroprotective response that supports lesion repair [24–27]. However, an alternative scenario is suggested by the observation that FGF9 is also upregulated in the serum and hippocampal tissue from patients with major depressive disorder (MDD) and in animal models of depression [28–30]. Intriguingly depression is not only a frequent co-morbidity in MS with a reported prevalence two to four times higher than in the general population [31, 32] but is also associated with grey matter atrophy of the same frontotemporal brain regions as in MDD [33]. This led us to speculate grey matter atrophy and associated functional deficits in both MS and MDD may involve contributions from previously unrecognised effects of FGF9 on neuronal rather than glial function and survival.

We now present data supporting this hypothesis. Comparative profiling of the transcriptional response of myelinated CNS cultures revealed FGF9, but neither FGF1 nor FGF2 downregulates the

expression of neuronal gene networks related to synaptic maintenance and impulse propagation. This transcriptional response was replicated in primary cultures of cortical neurons where it was associated with a rapid block in the development of inducible neuronal spiking activity and ultimately neuronal cell death. Extending these studies to investigate the consequences of over-expressing FGF9 in adult rat cortex *in vivo* demonstrated this also initiates rapid neuronal cell death, resulting in axonal loss, secondary loss of myelin and, ultimately, chronically myelin-depleted lesions with neuroaxonal reduction that recapitulate part of the histopathological findings of grey matter lesions in progressive MS. Collectively, these data identify FGF9-mediated neuronal dysfunction and death as an inflammatory demyelination-independent mechanism that can contribute to neurodegeneration in MS.

MATERIALS AND METHODS

Animals

Lewis rats were purchased from Harlan-Winkelmann GmbH (Borchen, Germany), Wistar rats were provided by the animal facility of the Max Planck Institute for Experimental Medicine, Göttingen, and Sprague Dawley rats were purchased from Charles River (United Kingdom). All animals were maintained in accordance with regional, national and EU regulations concerning animal welfare in standard cages on a 12 h light–dark cycle with food and water *ad libitum*.

Cell and tissue culture

Neurosphere-derived astrocytes were generated as described previously [20, 23]. Briefly, post-natal Day 1 striata of several Sprague–Dawley rats were dissociated and cells resuspended in 20 ml neurosphere media (see [20]) supplemented with 20 ng/ml mouse submaxillary gland epidermal growth factor (EGF, R&D Systems) in a 75 cm³ tissue culture flask. After approximately 1 week, formed neurospheres were triturated and plated on PLL-coated cover slips in low glucose DMEM supplemented with 10% foetal bovine serum and cultured until they formed a confluent monolayer.

Rat myelinating cultures were then established from Sprague–Dawley rat spinal cords on embryonic day 15.5 (harvested and pooled from several embryonic litters) as described previously [20, 34]. Cultures were maintained at 37°C/7% CO₂ and fed every 2 days by replacing half the culture medium. Insulin was withdrawn from the culture medium from DIV 13 onwards to promote myelination. Cultures were treated with human FGF1 (PreproTech; ED₅₀ < 0.5 ng/ml), FGF2 (PreProTech; ED₅₀ < 0.1 ng/ml) or FGF9 (R&D Systems; ED₅₀ 1–5 ng/ml) from DIV18 as indicated in the text. Neuronal cultures were generated according to a modified method from [35] by digesting cortex of E15.5 Sprague–Dawley rats in 0.25% trypsin (Sigma) and 0.1% collagenase I (Invitrogen) after 15 min at 37°C the cells were dissociated and the single cell suspension was plated on PLL-coated

cover slips (0.1 mg in boric acid buffer pH 8.4) at a density of 40,000 (for staining) or 400,000 cells (for qPCR) per cover slip in 100 µl neuromedia (neurobasal media containing B27 supplement, 5,000 IU/ml penicillin, 5 µg/ml streptomycin and 2 mM L-Glutamine; all Gibco). After 2 h, non-adherent cells were removed, and adherent cells cultured in neuromedia (1 ml per 35 mm petri dish containing three coverslips). Cells were fed twice a week by replacing half of the media; on DIV13, treatment with 100 ng/ml FGF9 (or FGF1 or FGF2) was started for either 3 or 10 days as stated in the text. Neuronal purity was routinely assessed by immunofluorescence microscopy as >95%; the majority of contaminating cells were GFAP⁺ astrocytes (3.1% ± 1.9% of all cells at DIV13).

RNA extraction and microarray analysis

RNA was extracted from myelinating cultures grown in the presence or absence of FGF1, FGF2 or FGF9 (100 ng/ml) for 24 h or 10 days using Qiagen RNeasy Micro kits according to manufacturer's instructions. RNA quality and integrity were checked using an Agilent Bioanalyzer 6000 Nano LabChip platform. Total RNAs were labelled with biotin using Ambion[®] WT Expression Kits following the Affymetrix GeneChip[®] WT Terminal Labeling and Hybridization protocol. Processed RNA was then hybridised to Affymetrix GeneChip[®] Rat Gene 1.0 ST Arrays using manufacturer's protocols for the Fluidics Station 450 and then scanned on a Gene Array Scanner 3000-7G. Data analysis was carried out using Partek Genomics Suite (Version 6.6, Partek Inc., St. Louis, MO, United States) software. Control and Treatment (FGF1, FGF2 or FGF9) groups were generated with three replicates per group. This dataset has been deposited in the Gene Expression Omnibus database (<http://www.ncbi.nlm.nih.gov/geo/accession> number GSE52753) [20]. Probe set level data were normalised using the GCRMA normalisation method and summarised to transcript cluster level using One-Step Tukey's Biweight method. Differential expression analysis was carried out by performing a two-way ANOVA test on the normalised expression values. Differentially expressed gene lists were generated based on the ANOVA (fold change $\geq \pm 2.0$ at a FDR adjusted *p* value of <0.05). Principal component analysis (PCA), gene expression heat map, differential expression profile analysis, gene ontology enrichment and network analysis were performed with Searchlight2 [36]. Three differential expression workflows (Control vs FGF1, Control vs FGF2 and Control vs FGF9) and one multiple differential expression workflow (combining the three individual workflows) were generated. For genes with multiple probe sets, the probe set with the lowest *p* value was retained, and only annotated genes have been analysed. For selected differential expression profiles, gene ontology enrichment was performed using a standard hypergeometric test with Benjamini–Hochberg multisample correction (significance at *p*-BH, 0.05) and using the cellular component database (<http://geneontology.org/>). For PCA, all expression values were used and per gene *z* scores to reduce high expression bias; the heatmap was generated using per gene expression *z* scores and clustered with Spearman distances, mean agglomeration and re-ordering.

For the expression profile of genes specifically down regulated by FGF9, network plots were generated. Nodes in the network denote significant gene ontologies, with the colour intensity representing $-\log_{10} p$ value. Two nodes were connected by an edge where >50% of the genes in the two gene ontologies were the same. For clarity, singleton nodes were removed. The network layout was generated using the R package network, under default settings, and used a Fruchterman–Reingold force-directed layout algorithm.

Quantitative real-time PCR

RNA extraction was performed using the Qiagen RNeasy Micro kit according to manufacturer's instructions for myelinating cultures or using the PureLink RNA Mini Kit (Invitrogen) for neuronal cell cultures. RNA quality and integrity were checked using the Agilent Bioanalyzer 6000 Nano LabChip platform.

The Qiagen QuantiTect[®] Reverse Transcription Kit was used for cDNA synthesis, with the following cycling parameters: DNA wipeout step 42°C for 2 min, after adding primer mix, reverse transcriptase and reaction buffer and second cycle: 42°C for 20 min and then 95°C for 3 min. Real-time PCR was performed using 1X SYBR Green master mix (Applied Biosystems), 50 pmol/μl of each primer, 10 ng cDNA template and distilled water. Primers were designed using Primer 3 software [37] (http://biotools.umassmed.edu/bioapps/primer3_www.cgi), sequences were checked with BLAST (<http://blast.ncbi.nlm.nih.gov/Blast.cgi>) and primers were purchased from IDT, sequences are stated in the table.

The reaction was amplified in an Applied Biosystems Fast Real-Time PCR System (ABI 7500) as described [20]. The comparative CT method (or the 2-ΔCT method) [38, 39] was used to determine differences in gene expression. For statistical analysis, paired *t* test was performed on the mean ΔCT for each experimental repeat to test for significant changes induced by FGF9 treatment as compared to untreated controls.

Electrophysiology

One million/100 μl embryonic rat cortical cells from Wistar rats (E18) were seeded on multi electrode arrays (60 electrodes, 30 μm diameter TiN-MEA, Multi Channel Systems) coated with Poly-D-lysine (50 μg/ml, Sigma-Aldrich, P7886) and Laminin from Engelbreth-Holm-Swarm murine sarcoma basement membrane (25 μg/ml, L2020-1MG, Sigma-Aldrich). Prior to seeding, AAV9-hSyn-hChR2 (H134R)-EYFP (Addgene, 26973-AAV9) was added to the cells in a final concentration of 3.39×10^2 genome copies/cell (Addgene). Culture medium consisted of neuronal basal medium without phenol red and antibiotics (Gibco, 12348017) enriched with glutaMAX 1:400 (Gibco, 35050038), FGF2 10 ng/ml (Gibco, 13256029) and B27 Supplement 1:50 (Gibco, 17504044). Medium was filled up to 1 ml per well 4 h after seeding. For medium exchange, 0.5 ml was replaced on DIV3, DIV7 and DIV14. Electrical recording started on DIV18 with a

spontaneous activity recording for 5–10 min and subsequent stimulation by 30 light pulses (see below for details) in medium without additives (control, *t* = 0 h), followed by an exchange of 0.1 ml medium with either pure medium (control group) or medium with FGF9 (treatment group). In the latter case, a final concentration of 100 ng/ml FGF9 was obtained. Further recordings were performed after *t* = 30 min, *t* = 51 h and *t* = 109 h. After *t* = 51 h recordings, 0.5 ml medium (with/without FGF9 100 ng/ml) was replaced.

To probe neuronal activity within the incubator at 37°C, 8% CO₂ and 90% humidity action potentials were recorded by a MEA2100-System (Multichannel Systems, Reutlingen, Germany), which was placed on of a high-power LED (480 ± 10 nm). The stimulation regime consisted of 30 rectangular pulses for 1 s followed by 3 s pause as described earlier [40]. Data were sampled with at least 10 kHz and further analysed by the open-source software package Spyking Circus [41]. Template matching was performed with default parameters at a template width of 3 ms, a spike detection threshold of six times median absolute deviation (MAD) and a bandwidth filter [200, auto]. This liberal threshold was chosen to avoid missing spikes. The noise-triggered threshold crossings were excluded based on their symmetric waveform. Templates with large or small symmetry were considered to represent noise. Moderate symmetry templates (>15 and < 30) were considered true spikes. For average post-stimulus response curves, the trials were averaged using 40 bins with a width of 6.25 ms (Figure 2E). The cumulative spike count during the first 250 ms of each stimulus episode was used as a read-out of spiking activity.

Immunofluorescence microscopy

Myelinating or neuronal cultures were fixed with 4% paraformaldehyde (PFA) for 15 min at RT, permeabilised for 15 min with 0.5% Triton-X and blocked for at least 30 min in PBS/10% Horse serum/1% bovine serum albumin. Cells were then incubated with primary antibodies for 45 min and washed in PBS before secondary antibodies were applied (15 min in the dark). Thereafter, coverslips were washed with PBS followed by distilled water and mounted with Mowiol 4-88 (Calbiochem, United Kingdom) containing DAPI. The following primary antibodies were used: NeuN (1:400, rabbit IgG, Millipore), β-tubulin (1:200, mlgG_{2a}, Merck), SMI-31 (1:1,000, mouse IgG1, Biolegend), Z2 (1:500, MOG-specific, mouse IgG2a [42]), MAP 2 (1:300, rabbit IgG, abcam), NG2 (1:200, rabbit IgG, Millipore) and Olig2 (1:500, rabbit IgG, Millipore). Species and isotype-specific secondary antibodies labelled with Alexa Fluor 488 or Alexa Fluor 568 (Invitrogen) were used at 1:400. For quantitative analysis, 10 random images from each of the three coverslips were taken at 10X magnification (neurite density and myelination of myelinating cultures) or 20X magnification (neuronal cultures and NG2, Olig2 cell numbers for myelinating cultures) using an Olympus BX51 fluorescent microscope and Ocular software (QImaging). Neurite density, myelination, Olig2 and DAPI counts were automatically quantified using CellProfiler cell image analysis software [43]. The pipelines used in this study were

developed in house and are available at Github (<https://github.com/muecs/cp>). Axonal density of myelinating cultures was analysed with the help of Fiji using the normalised local contrast filter plugin followed by autothresholding the image, and the histogram function was used to calculate % SMI31 pixels in the image (method adopted from <https://github.com/BarnettLab/MyelinJ> and [44]). MAP 2 and NG2 cell counts were manually quantified in a blinded fashion.

Adeno-associated viral (AAV-6)-based vector as a tool to express FGF9

To investigate the influence of FGF9 on astrocytes, oligodendrocytes, de- and remyelination and neuroaxonal damage, a replication-deficient vector based on adeno-associated virus 6 (AAV-6), was used to overexpress this protein. The AAV-6 vectors were constructed by Dr Sebastian Kügler, Department of Neurology, UMG [45]. The genome of the control viral vectors consisted of the astrocyte-specific GFAP promoter and the cDNA for enhanced green fluorescent protein (EGFP). Note that these AAV-EGFP constructs contain a woodchuck hepatitis post-transcriptional control element (WPRE), which stabilises mRNA, resulting in a 2- to 10-fold higher rate of protein expression. The constructed vectors were propagated in 293 cells using a helper plasmid [46] and purified [47]. After dialysis, genome titres were determined, and purification and identification of infectious titres were performed [45].

Intracerebral stereotactic injection

Adult female Lewis rats (3 months of age) were intraperitoneally (*i.p.*) anaesthetised by injection of ketamine (60 mg/kg body weight) and xylazine (8 mg/kg body weight). After loss of consciousness, a rostro-caudal cut was performed to gain access to the skull. Next, the animal was mounted in a stereotactic device. A fine hole was drilled into the skull 1 mm caudal and 2 mm sagittal to the bregma, until only a thin layer of bone was left to avoid damage to the brain. The skull and the meninges were then carefully opened with a microdissecting knife. One microlitre adeno-associated virus (AAV) vector solution (containing 10^8 viral genomes) was injected stereotactically by a fine calibrated glass capillary into the cortex (1.5 mm depth). Furthermore, to mark the injection site, monastral blue was added. The solution was administered very slowly during a period of 3 min to avoid tissue damage. After injection, the capillary was carefully withdrawn, and the skin was sutured. Finally, the animals were euthanized for qPCR or perfused at various time points after injection and the tissues were processed for immunohistochemistry.

Histology and immunohistochemistry

The deparaffinised 2–3 μm sections were processed for Bielschowsky's silver impregnation, Nissl staining or immunohistochemistry (IHC).

For IHC, endogenous peroxidase was blocked by incubation of the sections with 3% H_2O_2 /methanol, followed by heat antigen retrieval (microwave) with citrate buffer (pH 6.0) or EDTA buffer (pH 8.5). Sections were furthermore blocked with 10% foetal calf serum (FCS) and incubated with primary antibodies against APP (Chemicon, 1:3,000, mouse), CNP (Covance, 1:200, mouse), FGF9 (Abcam, 1:400, rabbit), GFAP (Dako, 1:1,000, rabbit), Iba-1 (Wako, 1:1,000, rabbit), PLP (Biozol, 1:250, mouse), MAG (myelin-associated glycoprotein; kindly provided by C. Richter-Landsberg, Oldenburg and T.V. Waehndt, Göttingen [48], 1:1,000, rabbit), MOG (rat anti-myelin oligodendrocyte glycoprotein [MOG] antiserum, 1:1,000, rat), NeuN (Millipore, 1:200, mouse), NogoA (kindly provided by M. Schwab [49], 1:20,000, mouse), Olig2 (IBL, 1:300, rabbit) and SMI32 (Covance Inc., Princeton, NJ, United States, 1:7,000, mouse) overnight. This was followed by incubation with species-specific HRP-conjugated secondary antibodies for 1 h, developed with DAB, and counterstained with haematoxylin.

For myelin quantification, colour deconvolution software in ImageJ [50] was used to select the DAB staining within the lesions. After conversion to binary images, particle analysis was used to quantify DAB-positive staining areas. Cell densities (ED1, CD3, NogoA, Olig2, NeuN, SMI32, Nissl, TUNEL, FGF9 and GFAP), as well as APP⁺ swellings, were counted from at least six different areas of each lesion at 400X magnification using an ocular morphometric grid.

TUNEL assay and in situ hybridisation

To visualise DNA fragmentation, terminal deoxynucleotidyl transferase dUTP nick end labelling (TUNEL) was performed by applying TdT-labelling mix (tailing buffer, Digoxigenin-DNA, terminal transferase, CoCl₂ 25mM) for 1 h onto deparaffinised sections pre-treated with proteinase K at 37°C for 15 min. After careful washing (five times), 10% FCS in PBS was applied as a blocking buffer for 15 min. Alkaline phosphatase-conjugated anti-digoxigenin Fab-fragments (1:500) dissolved in 10% FCS in PBS were added for 1 h. The staining was developed with NBT/BCIP (74-nitro blue tetrazolium chloride [NBT, Roche], 5-bromo-4-chloro-3-indolyl phosphate [BCIP, Roche]) solution, followed by co-staining with MAP 2 (1:300, rabbit IgG, Abcam) primary antibody in 10% FCS in PBS overnight. After incubation with rabbit specific AP-conjugated secondary antibodies for 1 h, the slide was developed with FastRed for 20 min and counterstained with haematoxylin.

For PLP-in-situ hybridisation (ISH) deparaffinised sections were also pre-treated with proteinase K. In addition, after deparaffinisation, post-fixation with 4% PFA and incubation with HCl was performed. Before application of the PLP probe, sections were incubated in 0.5% acetic anhydride and chloroform. The hybridisation mix was added to the sections for initially 4 min at 95°C and followed by an overnight incubation at 65°C. An alkaline phosphatase (AP)-coupled anti-digoxigenin antibody was developed with an NBT/BCIP solution (Roche) over night for chromogenic visualisation.

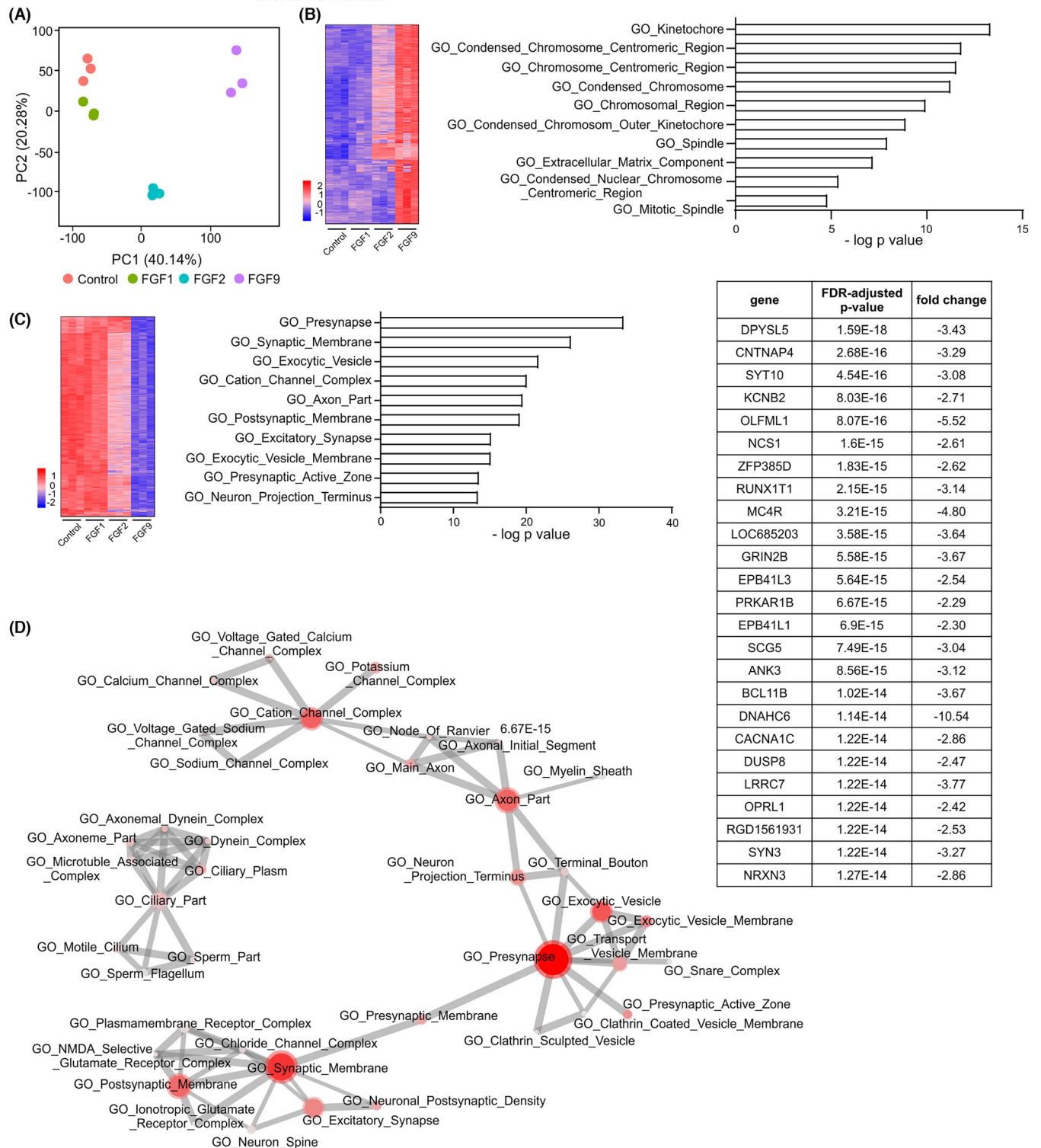


FIGURE 1 Legend on next page.

FIGURE 1 FGF9 down regulates gene networks required to maintain neuronal function. Myelinating rat CNS cultures were treated with 100 ng/ml FGF1, FGF2 or FGF9 for 10 days from DIV18 onwards and gene expression analysed using Affymetrix rat gene arrays. (A) Principal component analysis (PCA) shows PC1 (x axis), PC2 (y axis) and variance explained by each component; samples are coloured by sample group. (B, C) Differential expression profile analysis identified two transcriptional profiles specifically regulated by FGF9. (B) A subset of 565 genes up regulated associated with GO terms associated with cell division. (C) A subset of 881 down regulated genes associated with GO terms related to a synaptic/axonal phenotype. Gene expression heat map of transcripts with FDR adjusted $p < 0.05$ and fold change $> \pm 2$ for any of the FGF treatments (FGF1, FGF2 or FGF9) are shown. The heat maps show expression values for three replicates in each treatment group row-scaled into Z scores with colour intensities representing a range of expression values (high expression in red and low expression in blue). The y axis has been hierarchically clustered using spearman values and mean agglomeration. P values (hypergeometric test with Benjamini–Hochberg multisample correction) are provided for the 10 most significantly enriched GO terms for each profile, and shown are the 25 most significantly down regulated genes for expression profile in (C). (D) Network analysis of enriched GO terms for all 891 genes down regulated by FGF9 compared to untreated controls (FDR adjusted $p < 0.05$ and fold change > -2 vs control) indicates a detrimental effect on impulse transmission and transport processes.

Statistics

All experiments were performed a minimum of three times; biological replicates are defined as either different animals or independent cell cultures set up on different days from different animals. For in vitro data, technical replicates ($n = 3$) were set up for each condition on individual cover slips. Treatment groups were randomly assigned to cultures/animals, and data acquisition/analysis was performed blinded. All statistics were calculated with GraphPad Prism 7 (GraphPad Software Inc; La Jolla, CA, United States) using unpaired t test, paired t tests, one-way ANOVA or two-way ANOVA as specified in the text. A p value of < 0.05 was considered statistically significant, with **** $p < 0.0001$; *** $p < 0.001$; ** $p < 0.01$; * $p < 0.05$; n.s., not significant. Electrophysiological data have been analysed using the open-source stats package from the library SciPy 1.0 [51]. Prior to three-way ANOVA, the logarithm of rate values was taken after a small shift was applied (+1.5 Hz to account for zero rate responses) to achieve the precondition of normality on an ANOVA (Figure 2F, Supporting Information S2 ANOVA). A Shapiro Wilk test of the residuals of the ANOVA resulted in a p value of 0.28, thus not allowing to reject the Null hypothesis that the residuals are normally distributed. For post hoc comparison, a Mann–Whitney-U test was used with Bonferroni's multiple comparison correction.

RESULTS

FGF9 down regulates neuronal gene networks associated with synaptic function

A gene microarray study was performed on myelinating cultures treated with FGF1, FGF2 or FGF9 for 10 days (100 ng/ml; DIV 18–28). Three biological replicates were performed for each treatment and consistency between data sets confirmed by PCA (Figure 1A). We observed pronounced differences in the magnitude of the transcriptional response induced by these FGF family members. FGF1 differentially regulated expression of 35 genes (24 up regulated and 11 down regulated; FDR-adjusted $p < 0.05$ and ± 2 -fold cut off); FGF2 differentially regulated 431 genes (327 up regulated and 104 down regulated); and FGF9 differentially regulated expression of 1,465 genes

(574 up regulated and 891 down regulated) (Supporting Information S1 gene list).

Differential expression profile analyses of these data sets identified three transcriptional profiles with significantly enriched GO terms. Two were specific for FGF9, whilst the third was defined by 211 genes up regulated by FGF2 (Figure S1; Supporting Information S1 gene list). The profile defined by 565 genes up regulated by FGF9 was enriched in GO terms related to its mitogenic properties (Figure S2). However, the profile defined by 881 down regulated genes (Figure 1C; Supporting Information S1 gene list) was enriched in terms relating to neuronal function that included the GO terms Presynapse, Presynaptic Active Zone, Excitatory Synapse, Postsynaptic Membrane and Axonal Part (Figure 1C). This indicates FGF9 negatively affects neuronal function, an interpretation supported by network analysis of all genes down regulated by FGF9 compared to untreated control cultures (Figure 1D). This also identified multiple terms related to down regulation of synaptic function but revealed these are embedded in a more extensive network of interactions related to the function and maintenance of myelinated axons (GO Terms: Myelin sheath, Axon initial segment, Node of Ranvier; coordinated propagation of axonal action potentials [GO Terms: Cation Channel Complex, Voltage-gated Sodium Channel Complex, Voltage-gated Calcium Channel Complex, Potassium Channel Complex, Sodium Channel Complex]) and a second network indicative of dysregulation of microtubule function (GO Terms: Microtubule Associated Complex, Dynein complex, Ciliary Part) (Figure 1D).

FGF9 compromises neuronal survival and function

To investigate the neurodegenerative potential of FGF9, we first explored its effects on neurite density in myelinated cultures. Treatment with FGF9 (DIV 18–38) resulted in some reduction in neurite density compared to untreated controls ($p = 0.0056$; Figure 2A). To determine if this was a cell autonomous response or secondary effect of FGF9 on astrocytes and oligodendrocytes [20], we treated primary cultures of post-mitotic cortical neurons with FGF9 for 2 days (DIV 21–23). FGF9 rapidly down regulated neuronal gene expression in these cultures to a similar extent as seen in myelinating cultures (Table 1). To determine if this transcriptional response was associated

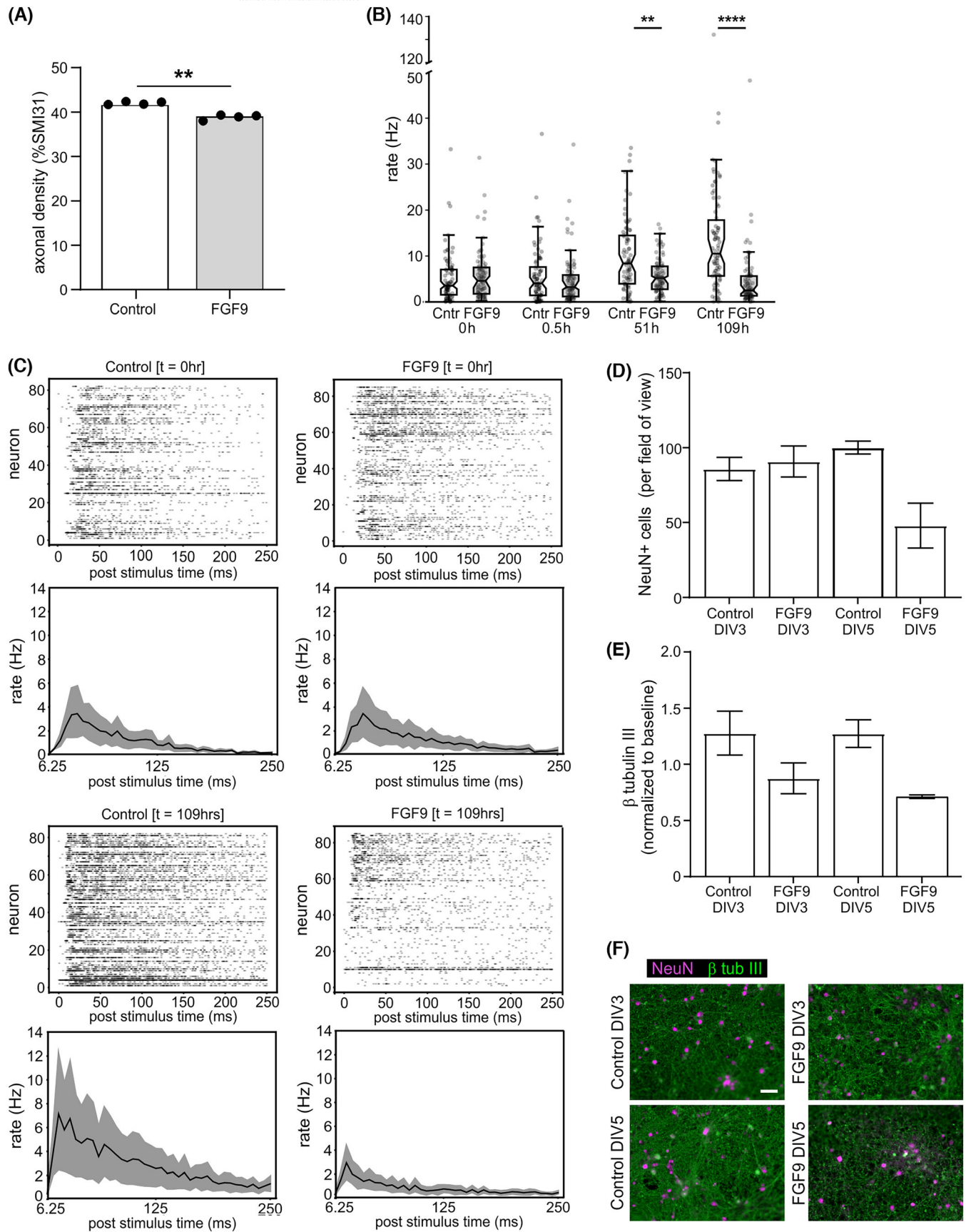


FIGURE 2 Legend on next page.

FIGURE 2 FGF9 compromises neuronal function and survival. Rat myelinating spinal cord cultures were treated with 100 ng/ml FGF9 from DIV18 on for 20 days, and neurite density (A, % of SMI31) was analysed by immune fluorescent microscopy; paired *t* test of FGF9 treated cultures compared to control shows a significant decrease in axonal density $**p < 0.01$. (B/C) Cultures of postmitotic cortical neurons were treated with 100 ng/ml FGF9 for 0.5, 51 and 109 h; spike raster plots from two representative electrodes before and 109 h after treatment with FGF9 (C). Displayed are the first 250 ms after stimulation onset for all 30 repetitions of the stimulus and the corresponding mean post-stimulus response curve with 95% CI (bootstrapped of 100 resamples). (B) Mean electrode responses of the first 250 ms post stimulus onset from 30 repetitions from different multi electrode arrays ($n_{MEA} = 3$ per group, all active electrodes control: $n_{electrode} = 82$ and FGF9: $n_{electrode} = 85$). Post hoc multiple comparison corrected by Bonferroni method revealed significant increase of activity in the control group both over time and compared to the treatment of FGF9 (100 ng/ml); for details, see [supporting information](#) ANOVA. Boxplots are presented according to standard Tukey's definition, whilst notches show 95% CI intervals (bootstrapped of 1,000 resamples). $**p < 0.01$; $****p < 0.0001$ (D–F) Neuronal cultures were treated with 100 ng/ml FGF9 for 3 or 5 days. Short-term FGF9 treatment had no effect on neuronal numbers (D: NeuN⁺ cells) and neurite density (E: β tubulin III), shown are mean \pm SEM. (F) Representative images for untreated (control) cultures or cultures treated with FGF9 for 3 days are shown; scale bars represent 50 μ m.

TABLE 1 Expression data for neuronal genes in myelinating cultures and primary cortical neurons

Gene	Myelinating cultures Fold change (p-value)		Cortical neurons Fold change (p-value)		Primer sequence
	Array	qPCR	qPCR	qPCR	
<i>Nefh</i>	−6.09	−2.42 \pm 0.5*	−3.3 \pm 1.0*		AGGACACAGGGTTAGCAACGTCACTAGCAGGGTGCGCTTTG
<i>Dnah9</i>	−6.99	−3.35 \pm 0.8*	−2.6 \pm 0.3**		CAAAGGGATGCTGGAGCAGATCACTTCGTTGTGGCTCTCC
<i>Sv2b</i>	−4.74	−3.79 \pm 0.6**	−2.6 \pm 0.4*		CTCTACCGCTGAATCGCTCGTTTGACAAGGTGCGTCCGGAG
<i>Kif5a</i>	−2.81	−3.07 \pm 0.9*	−2.6 \pm 0.3**		GGCCAGAGCAGAGATCACATTCTCCGACAGGTCA GCAAGAC
<i>Dnahc6</i>	−10.54	−3.97 \pm 1.3*	−13.1 \pm 2.9**		TGCAGAACGAGTGCAGTCAAAGAGCCGAAAGTGCCTTG
<i>Rbfox3</i>	−2.78	−3.01 \pm 0.4**	−3.8 \pm 1.0**		TCTATGCAGTGACCAGTTTCCC CCACGGGACTGGCA TTTTAAC
<i>Dync1i1</i>	−3.53	−2.86 \pm 0.7*	−2.6 \pm 0.4**		CCGTCCAGATGACTCCGATCAGCGGCTGCACTAGAGG

Note: Fold change for Control vs FGF9 for 48 h (cortical neurons) or 10 days (myelinating cultures) treatment with FGF9, *p* values for Δ Ct of Control vs FGF9 (*t* test), data from at least four independent experiments.

**p* < 0.05.

***p* < 0.01.

with a functional deficit, we performed multi electrode array measurements on cortical cell cultures. These were transduced with a commercially available viral construct encoding ChR2(H134R) under the control of a hSyn promoter that enabled us to drive neuronal spiking activity by short exposure to blue LED whole field stimulation. As previous experiments revealed spiking activity develops from around 14 DIV in this culture system, we elected to wait a further 4 days (DIV18, *t* = 0 h) to ensure robust readouts when treating cultures with FGF9 (Figure 2B,C).

Untreated control cultures showed an increase in light-driven neuronal activity from 5.1 Hz at *t* = 0.5 h to 10.0 Hz and 14.2 Hz at *t* = 51 h and *t* = 109 h (for confidence intervals, see Figure 2B), an increase analogous to that observed for spontaneous activity in similar cultures [52]. This increase in light-driven neuronal activity was abolished completely by FGF9, the frequency of spiking activity remaining unchanged from that observed in DIV18 control cultures (Figure 2B). Exemplary spike raster plots documenting this effect are shown in Figure 2C. Since synaptogenesis is the underlying cause of increased spiking activity in these cultures [53], our data imply FGF9 disrupts formation of new functional synapses, an interpretation supported by our transcriptomic data demonstrating FGF9 down regulates

expression of multiple genes contributing to synaptogenesis (Figure 1; Supporting Information S1 gene list). This rapid effect on light-driven neuronal activity seen after 51 h was not due to neuronal loss, as there was no significant decrease in NeuN⁺ cells in the first 72 h (Figure 2D–F). However, longer term exposure to FGF9 did compromise neuronal survival as after 10 days, the number of MAP2⁺ neurons was reduced by 50% (*p* = 0.0159), an effect accompanied by a 46% decrease in neurite density (*p* = 0.0057) compared to untreated controls (Figure S3).

FGF9 induces neurodegeneration and myelin loss in the adult rat cortex

To address the in vivo relevance of our in vitro observations, we injected adeno-associated viral vectors (AAV) encoding FGF9 or EGFP (enhanced green fluorescent protein) under control of a GFAP promoter into the motor cortex of naïve Lewis rats. qPCR analysis confirmed AAV-FGF9 mediated sustained expression of mouse *Fgf9*. Expression was highest at day 10 p.i. and then declined, although enhanced expression was still apparent 7 months p.i. (Figure S4).

Neither vector had any discernible effect on expression of rat *Fgf9* demonstrating tissue damage associated with the needle track had no effect on expression of endogenous rat *Fgf9* (Figure S4). The maximal fold-increase in *Fgf9* induced following injection of AAV-FGF9 is in the same range as that reported across some MS lesions [20, 21].

Local over-expression of FGF9 resulted in chronic lesions characterised by extensive loss of neurites and neurons, ensuing myelin loss, and associated with recruitment/activation of microglia/macrophages and astrocytosis (Figures 3, 4, and S5). We observed acute axonal transport disturbance as assessed by APP immunohistochemistry

(Figure 3A,B) and loss of axons by Bielschowsky silver impregnation (Figure 3C,D). Axonal pathology continued to accumulate throughout the study period. The number of APP positive spheroids, a marker for acute axonal injury [54], increased significantly between 3 and 9 months p.i. (Figure 3A,B) and was accompanied by a progressive decrease in axons identifiable by silver staining over the same time period, the latter indicating approximately 80% of axons were lost after 9 months (Figure 3C,D). Myelination as assessed by loss of immunohistochemical reactivity for myelin proteins declined to approximately 50% of control values after 1 month before plateauing

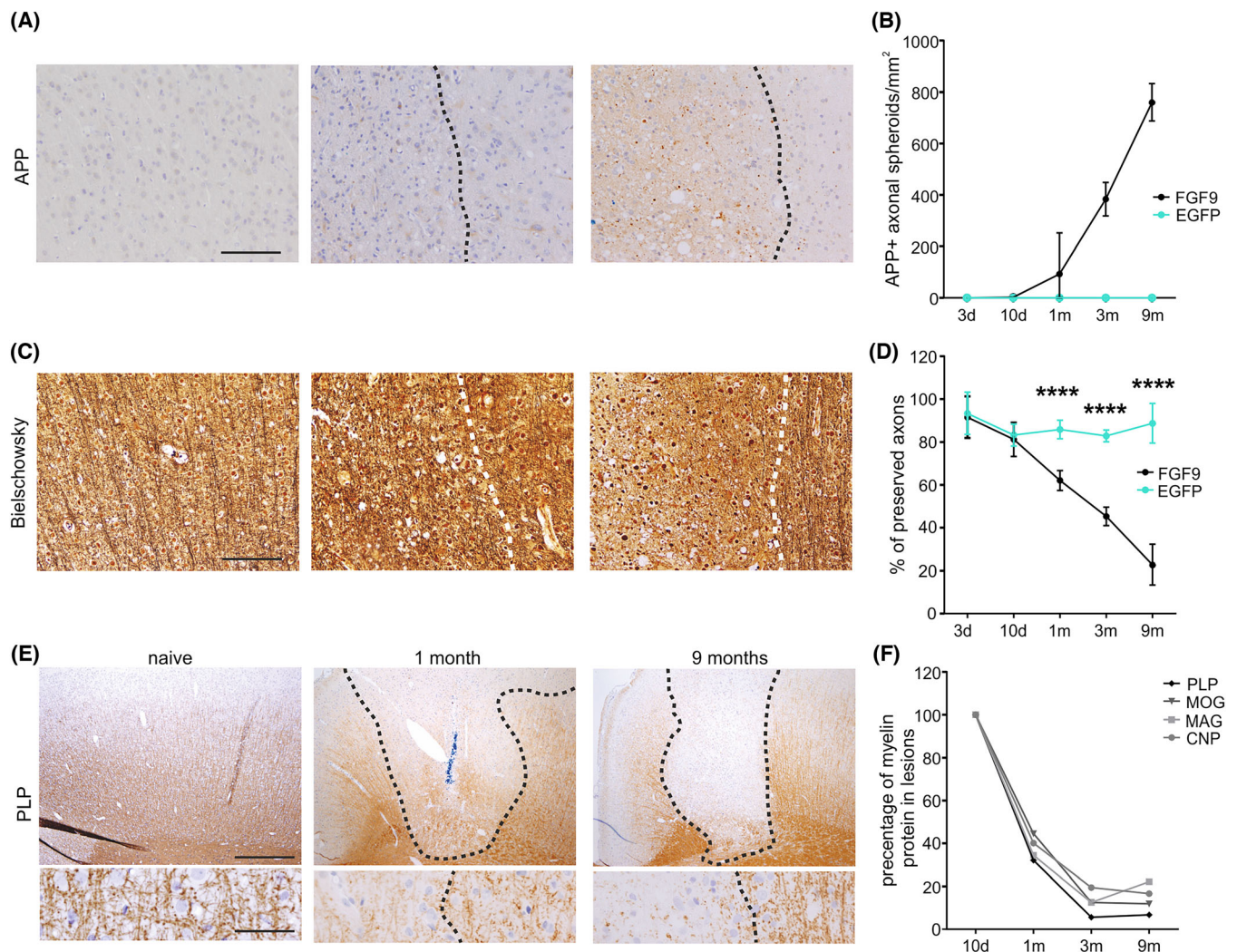


FIGURE 3 Over expression of fibroblast growth factor 9 (FGF9) induces progressive loss of axons and myelin in the rat cortex. (A, B) Immunohistochemistry for amyloid precursor protein (APP; brown). The number of APP positive spheroids increases progressively from 1 month post injection onwards in AAV-FGF9 induced lesions. Number of APP positive axonal spheroids is plotted as mean \pm SD ($n \geq 3$) for each time point and treatment group. Note: In the AAV-EGFP group, no APP positive spheroids were detected at any time point; scale bars, 500 µm. (C, D) Bielschowsky silver impregnation demonstrates accumulation of APP positive spheroids is associated with a corresponding loss of axons. $****p < 0.0001$ (two-way ANOVA followed by Šidák's post-test, mean \pm SD), scale bars, 500 µm. Dashed line marks the lesion border, lesion on the left. (E) Immunohistochemical (IHC) staining for proteolipid protein (PLP, brown). PLP immune reactivity declines progressively in AAV-FGF9 induced lesions until almost completely lost at 9 months. Scale bars, 500 µm (top panel) and 50 µm (bottom panel). (F) Immunohistochemical quantification of four myelin proteins (PLP, MOG [myelin oligodendrocyte glycoprotein], MAG [myelin-associated glycoprotein], CNP [2',3'-Cyclic-nucleotide 3'-phosphodiesterase]) within the lesion area reveals loss of myelin associated immune reactivity plateaus after 3 months. Note: No change in myelin protein associated immune reactivity was detected 10 days post injection. Shown is mean expression of four different myelin proteins within lesions compared to surrounding tissue (for each myelin protein $n = 2-4$ per time point).

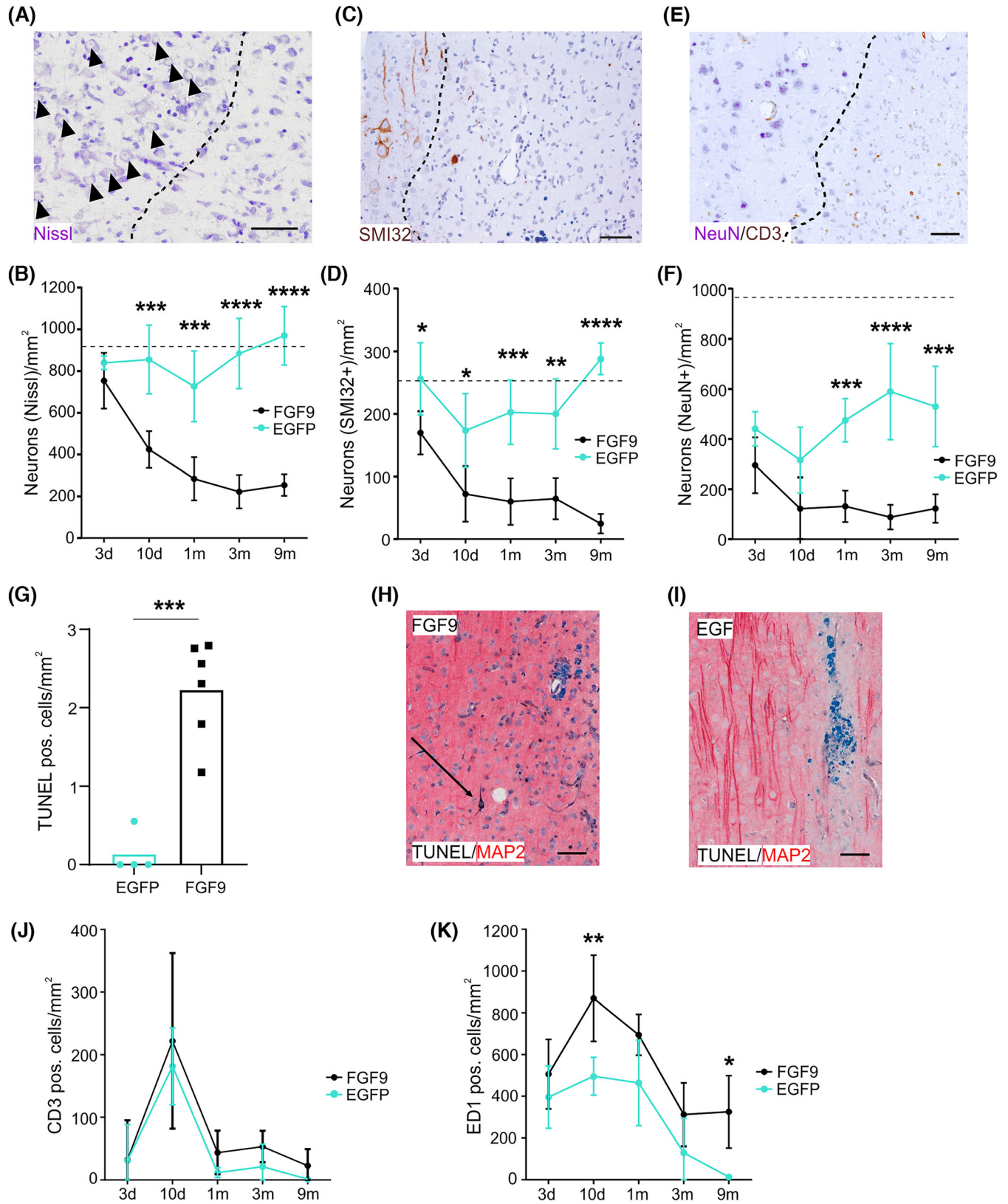


FIGURE 4 Legend on next page.

FIGURE 4 Over expression of FGF9 rapidly induces neuronal loss in the motor cortex. (A–F) Changes in neuronal density were quantified using three different methods (A, B: Nissl staining; C, D: non-phosphorylated neurofilament immune reactivity [SMI32]; E, F: NeuN immune reactivity). (A, C, E) Representative images across the lesion border (dotted line, lesion on the right side) 10 days after injection of AAV-FGF9. Scale bar, 50 μ m. (B, D, F) Neuronal density decreases rapidly following injection of AAV-FGF9 (Black) compared to AAV-EGFP controls (Turquoise). (G) Cell death, as assessed by TUNEL positive cells within the lesion, is significantly increased 5 days after injection of AAV-FGF9 compared to AAV-EGFP injected controls; $***p = 0.0003$, unpaired *t* test. (H, I) Representative image of TUNEL+ MAP 2+ neurons 5 d.p.i., TUNEL black, MAP 2 red; Scale bar, 50 μ m. (J) Quantification of CD3+ T cells in AAV-FGF9 and AAV-EGFP injected animals. (K) Quantification of ED1+ positive activated microglia/macrophages AAV-FGF9 and AAV-EGFP injected animals. (B) $***p = 0.0005$, $****p < 0.0001$; (D) $*p = 0.0159$, $*p = 0.0139$, $***p = 0.0007$, $**p = 0.0012$, $****p < 0.0001$; (F) $***p = 0.0002$, $****p < 0.0001$, $***p = 0.0001$; (K) $**p = 0.0051$, $*p = 0.0366$; two-way ANOVA followed by Šidák's post-test. Mean \pm SD.

at 10–20% of control values 2 months later (Figure 3E,F). Residual immune reactivity for myelin proteins at these later time points was found to be due to a combination of factors including the presence of myelin debris, myelin protein expression by cells of the oligodendrocyte lineage and aberrant (re)myelination (Figure S6).

We then strived to determine the precise relationship between axonal and myelin pathology and to elucidate whether loss of axons and myelin was a consequence of FGF9-mediated neuronal loss. Quantifying neuronal density by Nissl staining and immune reactivity for SMI32 (non-phosphorylated neurofilament) and NeuN demonstrated AAV-FGF9 caused an early and rapid decrease in neuronal density in comparison to AAV-EGFP injected controls (Figure 4A–F). At 10 days, neuronal loss was 50.4% ($p = 0.0005$), 58.5% ($p = 0.0139$) and 61.3% ($p = 0.076$) as assessed by Nissl staining and cellular immune reactivity for SMI32 and NeuN, respectively. Loss of neurons then slowed considerably, but after 9 months, neuronal density was reduced to 26.2% ($p < 0.0001$, Nissl staining), 8.6% ($p < 0.0001$, SMI32+ cells) and 23.2% ($p = 0.0001$, NeuN+ cells) of control values (Figure 4B,D,F). Neuronal pathology is therefore an early event in development of AAV-FGF9-induced lesions, which precedes axonal loss and demyelination. This interpretation is supported by our identification of a significant increase in the number of TUNEL+ MAP 2+ neurons 5 days p.i. (Figure 4G–I).

Grey matter lesions in progressive MS are characterised by demyelination and a reduction of neurons and neurites in association with activated microglia but in the absence of relevant numbers of T cells recruited from the periphery [55]. We therefore stained tissue sections to identify infiltrating CD3+ T cells and ED1+ macrophages and activated microglia. AAV-FGF9-induced lesions were not associated with increased recruitment of CD3+ T cells compared to AAV-EGFP injected controls at any time point (Figure 4J). However, early loss of neurons in AAV-FGF9 lesions was accompanied by a rapid increase in ED1+ macrophages/activated microglia (Figure 4K). ED1+ cell numbers peaked at 10 days but remained elevated for 9 months compared to AAV-EGFP controls.

DISCUSSION

Deciphering the mechanistic basis of neurodegeneration in MS is essential if we are to develop treatments to halt accumulation of disability in patients with longstanding progressive disease. In this

context, neuronal pathology is generally attributed to axonal injury and loss caused by repeated or sustained episodes of inflammatory demyelination. However, there is increasing evidence neuronal pathology not only occurs independently of demyelination but may also play a primary role in lesion development [10–12, 14, 15, 56, 57]. We now identify FGF9 as a factor up regulated in MS lesions [20] that compromises neuronal survival *in vivo*, thus making it a candidate molecule contributing to neuroaxonal demise in MS.

FGF9 is up regulated by oligodendrocytes and astrocytes at sites of ongoing tissue damage in MS [20, 21], where it was initially posited to exacerbate disease activity by inhibiting remyelination and/or up regulating expression of pro-inflammatory chemokines or alternatively suppress disease progression by providing some degree of neuroprotection [20]. The latter outcome was suggested by reports FGF9 mediates neuroprotection in cellular models of Parkinson's and Huntington's disease [58–60]. However, this scenario is now considered unlikely, as our new data demonstrate increased availability of FGF9 compromises neuronal survival *in vivo*. This effect was characterised by a rapid increase in neuronal apoptosis leading to extensive loss of neurons associated with axonal degeneration and secondary demyelination. Neuronal apoptosis increased significantly within 5 days, indicating that even transient, short-lived increases in FGF9 availability may have lasting effects on connectivity in the adult nervous system. These observations identify FGF9-mediated neurotoxicity as a potential mechanism contributing to demyelination-independent neuronal pathology in MS [9–15, 61].

Unravelling the pathways by which FGF9 compromises neuronal function and survival is now a major focus of research in our laboratories, but important clues can already be gleaned from data presented in this study. This goal is complicated by the multiplicity of mechanisms that regulate FGF signalling and its functional pleiotropy in terms of biological outcome in the CNS. Signal transduction in the CNS is mediated by three transmembrane receptor tyrosine kinases (FGFR1, FGFR2 and FGFR3), one or more of which are expressed by virtually all neurons and glial cells [62–65]. Moreover, each receptor can be activated by multiple FGF family members, albeit with strikingly different efficacies to initiate down-stream signalling by a variety of pathways including RAS-MAPK, PI3K-AKT, PLC γ and signal transducer and activator of transcription (STAT) [66]. In view of this complexity, we were surprised by the marked difference in the transcriptional response induced by FGF1

(35 differentially regulated genes), FGF2 (431 differentially regulated genes) and FGF9 (1465 differentially regulated genes) in myelinated cultures. Why this was the case remains unclear, but it may reflect cell specific differences in FGFR expression [67], differential modulation of feedback loops regulating FGF signalling pathways [66] or differences in the stability/biological half-lives of the recombinant FGFs used in this study. However, data generated using two other experimental platforms (cortical neuronal cultures; over expression in vivo) confirmed increased availability of FGF9 can indeed compromise neuronal function and/or survival. Moreover, these data were generated using three different rat strains (Sprague–Dawley, Wistar and Lewis) indicating this is a common, rather than strain-specific response to FGF9.

Mechanistically, our transcriptomic studies suggest FGF9 (directly or indirectly) acts to disrupt axonal transport. We believe this underlies the rapid block FGF9 places on the developmental increase in induced spiking activity in cortical neuronal cultures. Transport of synaptic components is mediated by interactions involving kinesin motors, whilst dynein motors mediate transport in the reverse direction [68]. FGF9 down regulates expression of both kinesin and dynein family members, indicating it will affect axonal transport in both directions [68, 69]. Such deficits play an integral role in other neurodegenerative diseases [68, 70] and are therefore likely to contribute to disruption of axonal transport [70–73] and synaptic pathologies reported in MS [10]. The clinical relevance of these observations is supported by studies indicating synaptic dysfunction plays an early role in MS [74–76]. Furthermore, mutations affecting expression and/or function of several genes down regulated by FGF9 are also associated with neurodegeneration including those encoding neurofilament subunits [77], motor proteins [78], KIF5a [79] and synaptic components such as Bassoon [80].

As FGFRs are expressed across all glial and neuronal lineages, it is difficult to untangle cell autonomous from off target effects of FGF9 [18]. A direct effect of FGF9 on neurons may be inferred from our experiments on primary cultures of cortical neurons. Expression of neuronal genes in these cultures was down regulated by FGF9 within 48 h, an effect associated with a block in developmental spiking behaviour that was statistically significant in the same time frame. This concept that enhanced FGF signalling is detrimental in neurons is supported by a recent study demonstrating introduction of a gain of function FGFR3 (the major receptor for FGF9) mutant into post-mitotic neurons results in severe tract abnormalities [63]. However, we should not neglect the possibility the neuronal response to FGF9 is an ‘off target’ effect of glial cell activation. FGF9 was identified originally as a ‘glial activating factor’ [81]. A recent study suggests neuronal FGF9 activates an astrocyte-dependent signalling network that contributes to modulation of astrocyte maturation, perineuronal net structure and synaptic refinement [82]. We cannot therefore exclude astrocyte-dependent responses contribute to the detrimental effects of FGF9 on neuronal function/survival reported in this study. Not only is astrocyte activation an early response in AAV-FGF9 induced lesions (Figure S5) but also our neuronal cultures contain a small number of residual GFAP⁺ astrocytes (~3% of cells per field of

view). We speculate the neuronal responses seen in this study involve contributions from mechanisms dependent on FGF9-signalling in neurons and astrocytes, enhanced and sustained FGFR activation being predicted to disrupt the normal homeostatic functions of FGF family members in the CNS [22]. Defining the cellular targets, FGFRs and effector pathways responsible for FGF9 mediated ‘neurotoxicity’ is now a matter of some urgency if we are to fully understand its role in MS and MDD.

Taken together, our observations demonstrate FGF9 compromises the functional integrity and survival of cortical neurons in vitro and initiates cortical neurodegeneration in vivo. In the living motor cortex, this results in chronic lesions that reproduce many features associated with cortical grey matter lesions in MS. Specifically, demyelination in both MS and AAV-FGF9 lesions is not only associated with transected neurites, apoptotic neurons and activated microglia [55] but also increased numbers of OPCs and pre-myelinating oligodendrocytes [83–86]. In AAV-FGF9-induced lesions, the density of Olig2⁺ cells and pre-myelinating NogoA⁺ oligodendrocytes increased five and two-fold respectively over 9 months (Figure S6). The soma of these oligodendrocytes was often swollen and exhibited a granular pattern of cytosolic immune reactivity for NogoA and MAG, whilst electron microscopy identified the presence of abnormal blebs and whorls of myelin (Figure S6). It is probable these pathologies are due to sustained over expression of FGF9 as they are consistent with data demonstrating FGF9 is not only an OPC mitogen (Figure S2), but in myelinating cultures results in the appearance of swollen pre-myelinating oligodendrocytes associated with blebs of myelin and which contain large cytoplasmic inclusions of myelin membrane-associated proteins [20]. Sustained over expression of FGF9 may account for these effects in late stage AAV-FGF9 lesions, but further studies are required to determine if this is also the case in MS.

Our previous data demonstrated FGF9 expression is restricted to a population of neurons in healthy brain but is strongly up regulated by glia in MS lesions [20]. Our experimental evidence indicates increased availability of FGF9 can contribute to lesion development via at least two distinct mechanisms; inhibition of remyelination [20] and as demonstrated in this study, rapidly compromising neuronal function and survival. The latter presumably plays a far more important role in development of grey matter lesions than those involving white matter tracts. However, how do our experimental studies relate to clinical studies on FGF9 in MS? Unfortunately, we are limited to transcriptional data, as no data are available on FGF9 concentrations in either MS tissue, sera or CSF. The biological significance of such data may anyway be of questionable value, as extracellular FGF9 is trapped by the extracellular matrix in and around MS lesions [20]. However, transcriptional data from a range of MS lesions [21, 87] do suggest the maximal fold changes in expression across lesions (compared to normal appearing white matter) is of a similar order to that induced by AAV-FGF9 in rat cortex (Day 10, approximately 50-fold; Day 30, approximately 30-fold, 7 months 10-fold) (Figure S4). It is clearly important not only to explore FGF9 expression and bioavailability in MS tissues in far greater detail but also to identify the

underlying mechanism driving FGF9 expression in MS lesions. The latter may involve virtual hypoxia, an important component of the pathophysiology of MS [88], as indicated from data obtained in relation to colonic cancer [89].

It is tempting to speculate these effects of FGF9 on neuronal functional and survival also contribute to loss of function in MDD in which FGF9 is up regulated in the hippocampus. Modelling this increase in experimental animals results in anxiety- and depression-like behaviours, whereas knocking down hippocampal FGF9 expression has the opposing effect [28]. Our data imply these behavioural effects are due to FGF9 compromising the function and/or survival of susceptible hippocampal neurons. Unfortunately, hippocampal pathology was not reported in the Aurbach study [28], and there is a paucity of detailed immunopathological studies of affected brain regions in MDD to support this hypothesis. Nonetheless, a recent study reported MDD is associated with reduced synaptic densities and synaptic gene expression in the prefrontal cortex [90]. The latter include *AMPH*, *CALM2*, *RAB3A*, *SYN1*, *SYN3* and *SYNGR3* all of which are also down regulated by FGF9 in myelinated cultures (Supporting Information S1 gene lists) [90]. Further studies are required to resolve the clinical significance of FGF9 mediated effects in MS and MDD, but our demonstration its overexpression triggers neurodegeneration raises the exciting possibility treatments designed to disrupt FGF signalling in other disorders may be repurposed to slow or even halt accumulation of disability.

AUTHOR CONTRIBUTIONS

Katja Thümmeler, Claudia Wrzos, Jonas Franz, Friedrich Schwarz, Daniel McElroy, John J. Cole, Lorna Hayden, Diana Arseni, Sebastian Kügler and Andreas Junker performed research and collected and analysed the data; Katja Thümmeler, Claudia Wrzos, Jonas Franz, Julia M. Edgar, Andreas Neef, Fred Wolf, Christine Stadelmann and Christopher Lington conceived and designed research and wrote the paper; Christine Stadelmann and Christopher Lington secured the funding.

ACKNOWLEDGEMENTS

Dr Michael Whitehead for providing the Fiji App to analyse axonal densities and Steve Muecklich for developing CellProfiler pipelines for automatic image quantification. We acknowledge the excellent technical support by Heidi Brodmerkel, Angela Dettmar, Bärbel Heidrich, Olga Kowatsch, Brigitte Maruschak, Uta Scheidt and Katja Schulz. We acknowledge support by the Open Access Publication Funds of the Göttingen University. We would like to thank Walter Stühmer for providing his laboratory for this study and creating an excellent scientific atmosphere. We acknowledge the excellent support of the Bernstein Center for Computational Neuroscience, University of Göttingen (J. F., A. N., and F. W.), and the Institute for Dynamics of Complex Systems, University of Göttingen (F. W.). Open Access funding enabled and organized by Projekt DEAL.

CONFLICT OF INTEREST STATEMENT

The authors declare no competing interests.

PEER REVIEW

The peer review history for this article is available at <https://www.webofscience.com/api/gateway/wos/peer-review/10.1111/nan.12935>.

DATA AVAILABILITY STATEMENT

The Microarray dataset has been deposited in the Gene Expression Omnibus database (<http://www.ncbi.nlm.nih.gov/geo/accession-number/GSE52753>). Software packages for fluorescence image analysis are available online (at <https://github.com/muecs/cp> and <https://github.com/BarnettLab/MyelinJ>) and for microarray data visualisation under Github (<https://github.com/Searchlight2/Searchlight2>).

ETHICS STATEMENT

All experiments were performed according to regional, national, and European regulations concerning animal welfare and animal experimentation and were authorised by the “Niedersächsische Landesamt für Verbraucherschutz und Lebensmittelsicherheit” (LAVES); grant number: 18–2760.

ORCID

Katja Thümmeler  <https://orcid.org/0000-0002-1681-2359>

REFERENCES

1. Kuhlmann T, Moccia M, Coetzee T, et al. Multiple sclerosis progression: time for a new mechanism-driven framework. *Lancet Neurol*. 2023;22(1):78–88. doi:10.1016/S1474-4422(22)00289-7
2. Carassiti D, Altmann DR, Petrova N, Pakkenberg B, Scaravilli F, Schmierer K. Neuronal loss, demyelination and volume change in the multiple sclerosis neocortex. *Neuropathol Appl Neurobiol*. 2018;44(4):377–390. doi:10.1111/nan.12405
3. Klaver R, de Vries HE, Schenk GJ, Geurts JGG. Grey matter damage in multiple sclerosis: a pathology perspective. *Prion*. 2013;7(1):66–75. doi:10.4161/pri.23499
4. Vercellino M, Masera S, Lorenzatti M, et al. Demyelination, inflammation, and neurodegeneration in multiple sclerosis deep gray matter. *J Neuropathol Exp Neurol*. 2009;68(5):489–502. doi:10.1097/NEN.0b013e3181a19a5a
5. Pravata E, Rocca MA, Valsasina P, et al. Gray matter trophism, cognitive impairment, and depression in patients with multiple sclerosis. *Mult Scler*. 2017;23(14):1864–1874. doi:10.1177/1352458517692886
6. Eshaghi A, Prados F, Brownlee WJ, et al. Deep gray matter volume loss drives disability worsening in multiple sclerosis. *Ann Neurol*. 2018;83(2):210–222. doi:10.1002/ana.25145
7. Friese MA, Schattling B, Fugger L. Mechanisms of neurodegeneration and axonal dysfunction in multiple sclerosis. *Nat Rev Neurol*. 2014;10(4):225–238. doi:10.1038/nrneurol.2014.37
8. Correale J, Marrodan M, Ysraelit MC. Mechanisms of neurodegeneration and axonal dysfunction in progressive multiple sclerosis. *Biomedicine*. 2019;7(1):14. doi:10.3390/biomedicine7010014
9. Trapp BD, Nave KA. Multiple sclerosis: an immune or neurodegenerative disorder? *Annu Rev Neurosci*. 2008;31(1):247–269. doi:10.1146/annurev.neuro.30.051606.094313
10. Albert M, Barrantes-Freer A, Lohrberg M, et al. Synaptic pathology in the cerebellar dentate nucleus in chronic multiple sclerosis. *Brain Pathol*. 2017;27(6):737–747. doi:10.1111/bpa.12450
11. Jürgens T, Jafari M, Kreutzfeldt M, et al. Reconstruction of single cortical projection neurons reveals primary spine loss in multiple sclerosis. *Brain*. 2016;139(Pt 1):39–46. doi:10.1093/brain/awv353

12. Trapp BD, Vignos M, Dudman J, et al. Cortical neuronal densities and cerebral white matter demyelination in multiple sclerosis: a retrospective study. *Lancet Neurol.* 2018;17(10):870-884. doi:10.1016/S1474-4422(18)30245-X
13. DeLuca GC, Williams K, Evangelou N, et al. The contribution of demyelination to axonal loss in multiple sclerosis. *Brain.* 2006;129(Pt 6):1507-1516. doi:10.1093/brain/awl074
14. Picon C, Jayaraman A, James R, et al. Neuron-specific activation of necroptosis signaling in multiple sclerosis cortical grey matter. *Acta Neuropathol.* 2021;141(4):585-604. doi:10.1007/s00401-021-02274-7
15. Schirmer L, Velmeshv D, Holmqvist S, et al. Neuronal vulnerability and multilineage diversity in multiple sclerosis. *Nature.* 2019;573(7772):75-82. doi:10.1038/s41586-019-1404-z
16. Deng Z, Deng S, Zhang MR, Tang MM. Fibroblast growth factors in depression. *Front Pharmacol.* 2019;10:60. doi:10.3389/fphar.2019.00060
17. Woodbury ME, Ikezu T. Fibroblast growth factor-2 signaling in neurogenesis and neurodegeneration. *J Neuroimmune Pharmacol.* 2014;9(2):92-101. doi:10.1007/s11481-013-9501-5
18. Guillemot F, Zimmer C. From cradle to grave: the multiple roles of fibroblast growth factors in neural development. *Neuron.* 2011;71(4):574-588. doi:10.1016/j.neuron.2011.08.002
19. Evans SJ, Choudary PV, Neal CR, et al. Dysregulation of the fibroblast growth factor system in major depression. *Proc Natl Acad Sci U S A.* 2004;101(43):15506-15511. doi:10.1073/pnas.0406788101
20. Lindner M, Thümmel K, Arthur A, et al. Fibroblast growth factor signalling in multiple sclerosis: inhibition of myelination and induction of pro-inflammatory environment by FGF9. *Brain.* 2015;138(Pt 7):1875-1893. doi:10.1093/brain/awv102
21. Mohan H, Friese A, Albrecht S, et al. Transcript profiling of different types of multiple sclerosis lesions yields FGF1 as a promoter of remyelination. *Acta Neuropathol Commun.* 2014;2:168.
22. Klimaschewski L, Claus P. Fibroblast growth factor signalling in the diseased nervous system. *Mol Neurobiol.* 2021;58(8):3884-3902. doi:10.1007/s12035-021-02367-0
23. Thümmel K, Rom E, Zeis T, et al. Polarizing receptor activation dissociates fibroblast growth factor 2 mediated inhibition of myelination from its neuroprotective potential. *Acta Neuropathol Commun.* 2019;7(1):212. doi:10.1186/s40478-019-0864-6
24. Ruffini F, Furlan R, Poliani PL, et al. Fibroblast growth factor-II gene therapy reverts the clinical course and the pathological signs of chronic experimental autoimmune encephalomyelitis in C57BL/6 mice. *Gene Ther.* 2001;8(16):1207-1213. doi:10.1038/sj.gt.3301523
25. Rottlaender A, Villwock H, Addicks K, Kuerten S. Neuroprotective role of fibroblast growth factor-2 in experimental autoimmune encephalomyelitis. *Immunology.* 2011;133(3):370-378. doi:10.1111/j.1365-2567.2011.03450.x
26. Yemisci M, Caban S, Gursoy-Ozdemir Y, et al. Systemically administered brain-targeted nanoparticles transport peptides across the blood-brain barrier and provide neuroprotection. *J Cereb Blood Flow Metab.* 2015;35(3):469-475. doi:10.1038/jcbfm.2014.220
27. Jin K, LaFevre-Bernt M, Sun Y, et al. FGF-2 promotes neurogenesis and neuroprotection and prolongs survival in a transgenic mouse model of Huntington's disease. *Proc Natl Acad Sci U S A.* 2005;102(50):18189-18194. doi:10.1073/pnas.0506375102
28. Aurbach EL, Inui EG, Turner CA, et al. Fibroblast growth factor 9 is a novel modulator of negative affect. *Proc Natl Acad Sci U S A.* 2015;112(38):11953-11958. doi:10.1073/pnas.1510456112
29. Wang XQ, Li WH, Tang YH, et al. The correlation between adiponectin and FGF9 in depression disorder. *Brain Res.* 2020;1729:146596. doi:10.1016/j.brainres.2019.146596
30. Li A, Tian J, Yang J, Ren X, Zhou Z, Zhou W. Expression of fibroblast growth factor 9 and its receptors in the dentate gyrus of hippocampus in poststroke depression rats. *Neuroreport.* 2021;32(4):321-325. doi:10.1097/WNR.0000000000001591
31. Boeschoten RE, Braamse AMJ, Beekman ATF, et al. Prevalence of depression and anxiety in multiple sclerosis: a systematic review and meta-analysis. *J Neurol Sci.* 2017;372:331-341. doi:10.1016/j.jns.2016.11.067
32. Patten SB, Marrie RA, Carta MG. Depression in multiple sclerosis. *Int Rev Psychiatry.* 2017;29(5):463-472. doi:10.1080/09540261.2017.1322555
33. van Geest Q, Boeschoten RE, Keijzer MJ, et al. Fronto-limbic disconnection in patients with multiple sclerosis and depression. *Mult Scler.* 2019;25(5):715-726. doi:10.1177/1352458518767051
34. Elliott C, Lindner M, Arthur A, et al. Functional identification of pathogenic autoantibody responses in patients with multiple sclerosis. *Brain.* 2012;135(Pt 6):1819-1833. doi:10.1093/brain/awt105
35. Schütze S, Loleit T, Zeretzke M, et al. Additive microglia-mediated neuronal injury caused by amyloid- β and bacterial TLR agonists in murine neuron-microglia co-cultures quantified by an automated image analysis using cognition network technology. *J Alzheimers Dis.* 2012;31(3):651-657. doi:10.3233/JAD-2012-120856
36. Cole JJ, Faydaci BA, McGuinness D, et al. Searchlight: automated bulk RNA-seq exploration and visualisation using dynamically generated R scripts. *BMC Bioinformatics.* 2021;22(1):411. doi:10.1186/s12859-021-04321-2
37. Rozen S, Skaletsky H. Primer3 on the WWW for general users and for biologist programmers. *Methods Mol Biol.* 2000;132:365-386.
38. Livak KJ, Schmittgen TD. Analysis of relative gene expression data using real-time quantitative PCR and the 2⁻(Delta Delta C [T]) method. *Methods.* 2001;25(4):402-408. doi:10.1006/meth.2001.1262
39. Schmittgen TD, Livak KJ. Analyzing real-time PCR data by the comparative C(T) method. *Nat Protoc.* 2008;3(6):1101-1108. doi:10.1038/nprot.2008.73
40. el Hady A, Afshar G, Bröking K, et al. Optogenetic stimulation effectively enhances intrinsically generated network synchrony. *Front Neural Circuits.* 2013;7:167.
41. Yger P, Spampinato GLB, Esposito E, et al. A spike sorting toolbox for up to thousands of electrodes validated with ground truth recordings in vitro and in vivo. *Elife.* 2018;7:7. doi:10.7554/eLife.34518
42. Piddlesden SJ, Lassmann H, Zimprich F, Morgan BP, Lington C. The demyelinating potential of antibodies to myelin oligodendrocyte glycoprotein is related to their ability to fix complement. *Am J Pathol.* 1993;143(2):555-564.
43. Carpenter AE, Jones TR, Lamprecht MR, et al. CellProfiler: image analysis software for identifying and quantifying cell phenotypes. *Genome Biol.* 2006;7(10):R100. doi:10.1186/gb-2006-7-10-r100
44. Whitehead MJ, McCanney GA, Willison HJ, Barnett SC. MyelinJ: an ImageJ macro for high throughput analysis of myelinating cultures. *Bioinformatics.* 2019;35(21):4528-4530. doi:10.1093/bioinformatics/bt403
45. Kügler S, Lingor P, Schöll U, Zolotukhin S, Bähr M. Differential transgene expression in brain cells in vivo and in vitro from AAV-2 vectors with small transcriptional control units. *Virology.* 2003;311(1):89-95. doi:10.1016/S0042-6822(03)00162-4
46. Grimm S, Voss-Neudecker F. High-purity plasmid isolation using silica oxide. *Methods Mol Biol.* 2003;235:83-87.
47. Malik JM, Shevtsova Z, Bähr M, et al. Long-term in vivo inhibition of CNS neurodegeneration by Bcl-XL gene transfer. *Mol Ther.* 2005;11(3):373-381. doi:10.1016/j.ymthe.2004.11.014
48. Matthieu JM, Waehndt TV, Eschmann N. Myelin-associated glycoprotein and myelin basic protein are present in central and peripheral nerve myelin throughout phylogeny. *Neurochem Int.* 1986;8(4):521-526. doi:10.1016/0197-0186(86)90186-5

49. Oertle T, van der Haar ME, Bandtlow CE, et al. Nogo-A inhibits neurite outgrowth and cell spreading with three discrete regions. *J Neurosci*. 2003;23(13):5393-5406. doi:10.1523/JNEUROSCI.23-13-05393.2003
50. Ruifrok AC, Johnston DA. Quantification of histochemical staining by color deconvolution. *Anal Quant Cytol Histol*. 2001;23(4):291-299.
51. Virtanen P, Gommers R, Oliphant TE, et al. SciPy 1.0: fundamental algorithms for scientific computing in Python. *Nat Methods*. 2020;17(3):261-272. doi:10.1038/s41592-019-0686-2
52. van Pelt J, Corner MA, Wolters PS, et al. Longterm stability and developmental changes in spontaneous network burst firing patterns in dissociated rat cerebral cortex cell cultures on multielectrode arrays. *Neurosci Lett*. 2004;361(1-3):86-89. doi:10.1016/j.neulet.2003.12.062
53. Muramoto K, Ichikawa M, Kawahara M, Kobayashi K, Kuroda Y. Frequency of synchronous oscillations of neuronal activity increases during development and is correlated to the number of synapses in cultured cortical neuron networks. *Neurosci Lett*. 1993;163(2):163-165. doi:10.1016/0304-3940(93)90372-R
54. Ferguson B, Matyszak MK, Esiri MM, et al. Axonal damage in acute multiple sclerosis lesions. *Brain*. 1997;120(Pt 3):393-399. doi:10.1093/brain/120.3.393
55. Peterson JW, Bö L, Mörk S, Chang A, Trapp BD. Transected neurites, apoptotic neurons, and reduced inflammation in cortical multiple sclerosis lesions. *Ann Neurol*. 2001;50(3):389-400. doi:10.1002/ana.1123
56. Barnett MH, Prineas JW. Relapsing and remitting multiple sclerosis: pathology of the newly forming lesion. *Ann Neurol*. 2004;55(4):458-468. doi:10.1002/ana.20016
57. Kassmann CM, Lappe-Siefke C, Baes M, et al. Axonal loss and neuroinflammation caused by peroxisome-deficient oligodendrocytes. *Nat Genet*. 2007;39(8):969-976. doi:10.1038/ng2070
58. Huang JY, Hong YT, Chuang JI. Fibroblast growth factor 9 prevents MPP⁺-induced death of dopaminergic neurons and is involved in melatonin neuroprotection in vivo and in vitro. *J Neurochem*. 2009;109(5):1400-1412. doi:10.1111/j.1471-4159.2009.06061.x
59. Kanda T, Iwasaki T, Nakamura S, Kurokawa T, Ikeda K, Mizusawa H. Self-secretion of fibroblast growth factor-9 supports basal forebrain cholinergic neurons in an autocrine/paracrine manner. *Brain Res*. 2000;876(1-2):22-30. doi:10.1016/S0006-8993(00)02563-4
60. Yusuf IO, Chen HM, Cheng PH, et al. Fibroblast growth factor 9 stimulates neuronal length through NF- κ B signaling in striatal cell Huntington's disease models. *Mol Neurobiol*. 2021;58(5):2396-2406. doi:10.1007/s12035-020-02220-w
61. Calabrese M, Magliozzi R, Ciccarelli O, Geurts JGG, Reynolds R, Martin R. Exploring the origins of grey matter damage in multiple sclerosis. *Nat Rev Neurosci*. 2015;16(3):147-158. doi:10.1038/nrn3900
62. Reuss B, Hertel M, Werner S, Unsicker K. Fibroblast growth factors-5 and -9 distinctly regulate expression and function of the gap junction protein connexin43 in cultured astroglial cells from different brain regions. *Glia*. 2000;30(3):231-241. doi:10.1002/(SICI)1098-1136(200005)30:3<231::AID-GLIA3>3.0.CO;2-1
63. Huang JY, Krebs BB, Miskus ML, et al. Enhanced FGFR3 activity in postmitotic principal neurons during brain development results in cortical dysplasia and axonal tract abnormality. *Sci Rep*. 2020;10(1):18508. doi:10.1038/s41598-020-75537-0
64. Fortin D, Rom E, Sun H, Yayon A, Bansal R. Distinct fibroblast growth factor (FGF)/FGF receptor signaling pairs initiate diverse cellular responses in the oligodendrocyte lineage. *J Neurosci*. 2005;25(32):7470-7479. doi:10.1523/JNEUROSCI.2120-05.2005
65. Young KM, Mitsumori T, Pringle N, Grist M, Kessar N, Richardson WD. An Fgfr3-iCreER(T2) transgenic mouse line for studies of neural stem cells and astrocytes. *Glia*. 2010;58(8):943-953. doi:10.1002/glia.20976
66. Ornitz DM, Itoh N. The fibroblast growth factor signaling pathway. *Wiley Interdiscip Rev Dev Biol*. 2015;4(3):215-266. doi:10.1002/wdev.176
67. Zhang Y, Chen K, Sloan SA, et al. An RNA-sequencing transcriptome and splicing database of glia, neurons, and vascular cells of the cerebral cortex. *J Neurosci*. 2014;34(36):11929-11947. doi:10.1523/JNEUROSCI.1860-14.2014
68. Bury LA, Sabo SL. Building a terminal: mechanisms of presynaptic development in the CNS. *Neuroscientist*. 2016;22(4):372-391. doi:10.1177/1073858415596131
69. Sleigh JN, Rossor AM, Fellows AD, Tosolini AP, Schiavo G. Axonal transport and neurological disease. *Nat Rev Neurol*. 2019;15(12):691-703. doi:10.1038/s41582-019-0257-2
70. Guo W, Stoklund Dittlau K, van den Bosch L. Axonal transport defects and neurodegeneration: molecular mechanisms and therapeutic implications. *Semin Cell Dev Biol*. 2020;99:133-150. doi:10.1016/j.semcdb.2019.07.010
71. van den Berg R, Hoogenraad CC, Hintzen RQ. Axonal transport deficits in multiple sclerosis: spiraling into the abyss. *Acta Neuropathol*. 2017;134(1):1-14. doi:10.1007/s00401-017-1697-7
72. Dendrou CA, Fugger L. Please mind the gap: axonal transport deficits in multiple sclerosis neurodegeneration. *Neuron*. 2014;84(6):1105-1107. doi:10.1016/j.neuron.2014.12.012
73. Sorbara CD, Wagner NE, Ladwig A, et al. Pervasive axonal transport deficits in multiple sclerosis models. *Neuron*. 2014;84(6):1183-1190. doi:10.1016/j.neuron.2014.11.006
74. Dutta R, Chang A, Doud MK, et al. Demyelination causes synaptic alterations in hippocampi from multiple sclerosis patients. *Ann Neurol*. 2011;69(3):445-454. doi:10.1002/ana.22337
75. Mandolesi G, Gentile A, Musella A, et al. Synaptopathy connects inflammation and neurodegeneration in multiple sclerosis. *Nat Rev Neurol*. 2015;11(12):711-724. doi:10.1038/nrneuro.2015.222
76. Petrova N, Nutma E, Carassiti D, et al. Synaptic loss in multiple sclerosis spinal cord. *Ann Neurol*. 2020;88(3):619-625. doi:10.1002/ana.25835
77. Didonna A, Opal P. The role of neurofilament aggregation in neurodegeneration: lessons from rare inherited neurological disorders. *Mol Neurodegener*. 2019;14(1):19. doi:10.1186/s13024-019-0318-4
78. Lipka J, Kuijpers M, Jaworski J, Hoogenraad CC. Mutations in cytoplasmic dynein and its regulators cause malformations of cortical development and neurodegenerative diseases. *Biochem Soc Trans*. 2013;41(6):1605-1612. doi:10.1042/BST20130188
79. Brenner D, Yilmaz R, Müller K, et al. Hot-spot KIF5A mutations cause familial ALS. *Brain*. 2018;141(3):688-697. doi:10.1093/brain/awx370
80. Schattling B, Engler JB, Volkmann C, et al. Bassoon proteinopathy drives neurodegeneration in multiple sclerosis. *Nat Neurosci*. 2019;22(6):887-896. doi:10.1038/s41593-019-0385-4
81. Santos-Ocampo S, Colvin JS, Chellaiah A, Ornitz DM. Expression and biological activity of mouse fibroblast growth factor-9. *J Biol Chem*. 1996;271(3):1726-1731. doi:10.1074/jbc.271.3.1726
82. Brandebura AN, Kolson DR, Amick EM, et al. Transcriptional profiling reveals roles of intercellular Fgf9 signaling in astrocyte maturation and synaptic refinement during brainstem development. *J Biol Chem*. 2022;298(8):102176. doi:10.1016/j.jbc.2022.102176
83. Strijbis EMM, Kooi EJ, van der Valk P, Geurts JGG. Cortical remyelination is heterogeneous in multiple sclerosis. *J Neuropathol Exp Neurol*. 2017;76(5):390-401. doi:10.1093/jnen/nlx023
84. Chang A, Tourtellotte WW, Rudick R, Trapp BD. Premyelinating oligodendrocytes in chronic lesions of multiple sclerosis. *N Engl J Med*. 2002;346(3):165-173. doi:10.1056/NEJMoa010994
85. Albert M, Antel J, Brück W, Stadelmann C. Extensive cortical remyelination in patients with chronic multiple sclerosis. *Brain Pathol*. 2007;17(2):129-138. doi:10.1111/j.1750-3639.2006.00043.x

86. Rodriguez EG, Wegner C, Kreutzfeldt M, et al. Oligodendroglia in cortical multiple sclerosis lesions decrease with disease progression, but regenerate after repeated experimental demyelination. *Acta Neuropathol.* 2014;128(2):231-246. doi:[10.1007/s00401-014-1260-8](https://doi.org/10.1007/s00401-014-1260-8)
87. Mohan H. Extracellular matrix and oligodendrocyte regulators in different types of multiple sclerosis lesions: implications for lesion development and regulation of remyelination, in https://edoc.ub.uni-muenchen.de/12467/2/Mohan_Hema.pdf. 2010.
88. Halder SK, Milner R. Hypoxia in multiple sclerosis; is it the chicken or the egg? *Brain.* 2021;144(2):402-410. doi:[10.1093/brain/awaa427](https://doi.org/10.1093/brain/awaa427)
89. Chen TM, Shih YH, Tseng JT, et al. Overexpression of FGF9 in colon cancer cells is mediated by hypoxia-induced translational activation. *Nucleic Acids Res.* 2014;42(5):2932-2944. doi:[10.1093/nar/gkt1286](https://doi.org/10.1093/nar/gkt1286)
90. Kang HJ, Voleti B, Hajszan T, et al. Decreased expression of synapse-related genes and loss of synapses in major depressive disorder. *Nat Med.* 2012;18(9):1413-1417. doi:[10.1038/nm.2886](https://doi.org/10.1038/nm.2886)

SUPPORTING INFORMATION

Additional supporting information can be found online in the Supporting Information section at the end of this article.

How to cite this article: Thümmeler K, Wrzos C, Franz J, et al. Fibroblast growth factor 9 (FGF9)-mediated neurodegeneration: Implications for progressive multiple sclerosis? *Neuropathol Appl Neurobiol.* 2023;49(5):e12935. doi:[10.1111/nan.12935](https://doi.org/10.1111/nan.12935)